Crystal Structures of Amylosucrase from *Neisseria polysaccharea* in Complex with D-Glucose and the Active Site Mutant Glu328Gln in Complex with the Natural Substrate Sucrose†

Osman Mirza,‡ Lars K. Skov,‡ Magali Remaud-Simeon,§ Gabrielle Potocki de Montalk,§ Cecile Albenne,§ Pierre Monsan,§ and Michael Gajhede*,‡

Protein Structure Group, Department of Chemistry, University of Copenhagen, Universitetsparken 5, DK-2100 Copenhagen, Denmark, and Institut National des Sciences Appliquees, INSA, DGBA, CNRS UMR 5504, INRA UMR792 135, Avenue de Rangueil 31077, Toulouse, France

Received April 6, 2001; Revised Manuscript Received May 29, 2001

ABSTRACT: The structure of amylosucrase from *Neisseria polysaccharea* in complex with β-D-glucose has been determined by X-ray crystallography at a resolution of 1.66 Å. Additionally, the structure of the inactive active site mutant Glu328Gln in complex with sucrose has been determined to a resolution of 2.0 Å. The D-glucose complex shows two well-defined D-glucose molecules, one that binds very strongly in the bottom of a pocket that contains the proposed catalytic residues (at the subsite −1), in a nonstrained $^4C_1$ conformation, and one that binds in the packing interface to a symmetry-related molecule. A third weaker D-glucose-binding site is located at the surface near the active site pocket entrance. The orientation of the D-glucose in the active site emphasizes the Glu328 role as the general acid/base. The binary sucrose complex shows one molecule bound in the active site, where the glucosyl moiety is located at the α-amylase −1 position and the fructosyl ring occupies subsite +1. Sucrose effectively blocks the only visible access channel to the active site. From analysis of the complex it appears that sucrose binding is primarily obtained through enzyme interactions with the glucosyl ring and that an important part of the enzyme function is a precise alignment of a lone pair of the linking O1 oxygen for hydrogen bond interaction with Glu328. The sucrose specificity appears to be determined primarily by residues Asp144, Asp394, Arg446, and Arg509. Both Asp394 and Arg446 are located in an insert connecting β-strand 7 and α-helix 7 that is much longer in amylosucrase compared to other enzymes from the α-amylase family (family 13 of the glycoside hydrolases).

Amylosucrase (AS) from *Neisseria polysaccharea* is a glucosyltransferase (EC 2.4.1.4) that catalyzes the transfer of a D-glucopyranosyl moiety from sucrose onto an acceptor molecule. When the acceptor is another saccharide, only α-1,4 linkages are produced. Unlike most amylopolysaccharide synthases, AS does not require any α-D-glucosyl nucleoside diphosphate substrate. In the presence of glycogen AS catalyzes the transfer of a D-glucose moiety onto a glycogen branch (*1*), but in the absence of glycogen the reaction pathway is more complex; here polymer synthesis, hydrolysis of sucrose, synthesis of smaller maltosaccharides, and synthesis of sucrose isoforms are observed (*2*). Hydrolysis is always just a minor side reaction. The function of AS in vivo is undoubtedly the extension of glycogen-like oligosaccharides, which is clearly demonstrated by the formidable increase in k_{cat} observed when glycogen is present (*1*).

On the basis of sequence similarities the enzyme has been placed in the retaining glycoside hydrolase family 13 according to Henrissat (*3*). Family 13 is the largest of all the families and contains mainly enzymes acting on starch, such as α-amylase and cyclodextrin glycosyltransferase (CGTase), but also enzymes specific for cleavage of other glucosidic linkages such as α-1,6 and α-1,1 bonds. It is widely believed that the catalytic mechanism in family 13 glycosidases occurs via a double displacement reaction, in which a covalent glycosyl-enzyme intermediate is formed (*4*−*7*). In a subsequent step this glucosyl moiety is transferred onto a water molecule (main reaction catalyzed by α-amylases) or onto a hydroxyl group from a sugar acceptor in a transglucosylation reaction. Both steps are suggested to proceed via oxocarbenium ion transition states (Figure 1). In particular CGTases reacts intramolecularly with the nonreducing end of the covalently linked heptasaccharide (*6*).

The sequence of AS contains the two catalytic acidic residues found in α-amylases, and they can be identified by sequence alignment (*8*). Single-site mutational studies of residues Asp286 and Glu328 (crystal structure numbering) showed in both cases a total inactivation of AS (*9*). Additionally, the mutation of three other active site residues

† This work was supported by the EU biotechnology project Alpha-Glucan Active Designer Enzymes (AGADE, BI04-CT98-0022), the Danish Natural Research Council, and the Danish Synchrotron User Center (DANSYNC).

* Corresponding author. Telephone: +45 35320280. Fax: +45 35320299. E-mail: gajhede@psg.ki.ku.dk.

‡ University of Copenhagen.

§ Institut National des Sciences Appliquees.

10.1021/bi010706l CCC: $20.00
Published on Web 07/06/2001

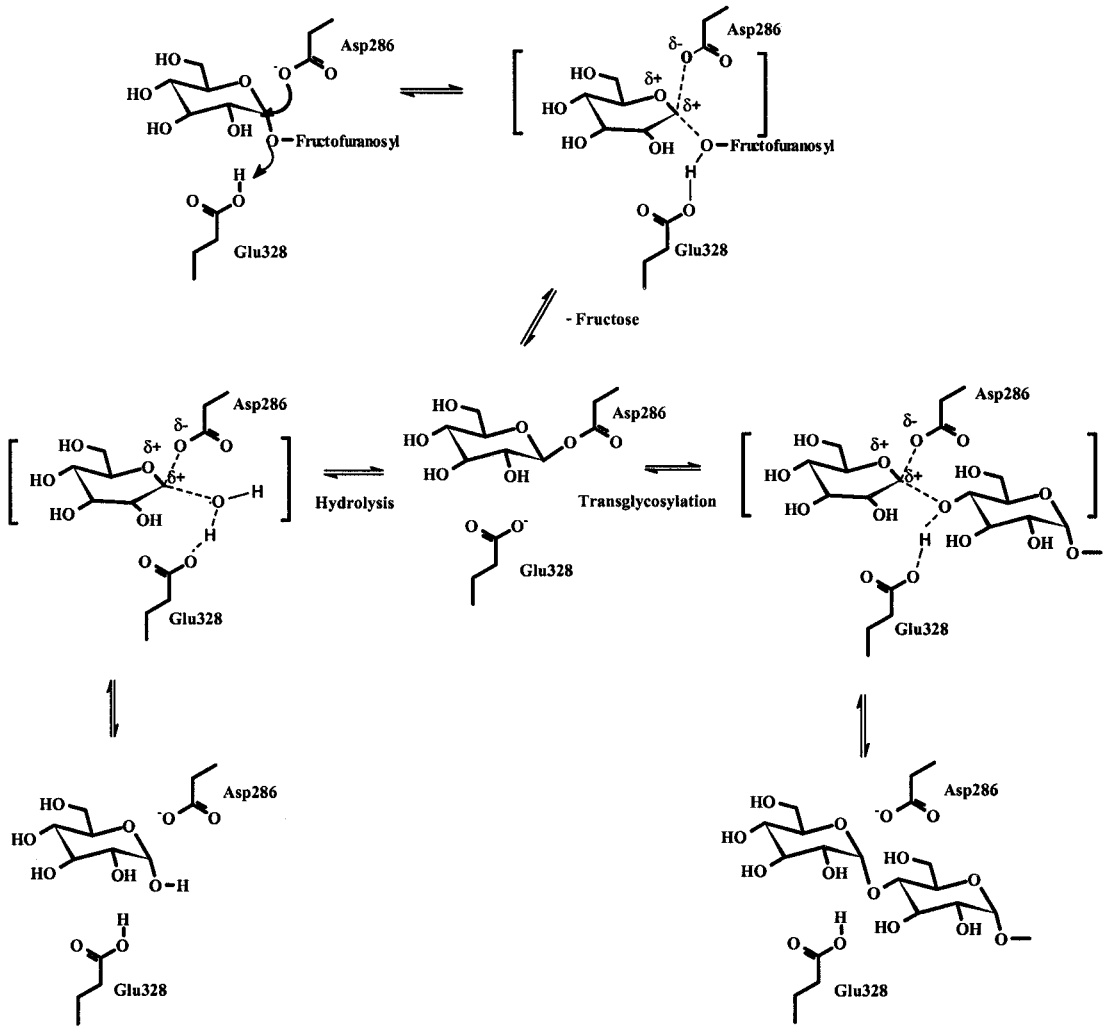

FIGURE 1: Schematic representation of the reaction pathway.

conserved in family 13 (Asp393, His187, and His392) resulted in a large decrease in activity.

Family 13 belongs to clan GH-H (*10*), which also contains family 70 including sucrose glucosyltransferases from *Leuconostoc sp.* (dextran sucrases and alternan sucrase), *Lactobacillus sp*., and *Streptococcus sp*. and family 77 including amylomaltase from *Thermus aquaticus* and 4-α-glucanotransferases from various bacteria. The basic structural framework for the enzymes of this clan is a catalytic core domain containing a $(\beta/\alpha)_8$ motif usually termed domain A.

The full-length AS consists of 636 amino acids, and the structure of the enzyme with Tris[1] bound in the active site has been reported recently by Skov et al. (*11*). The expected inhibitory effect of the Tris molecule has not yet been determined. A unique feature for AS is an N-terminal domain (termed N) consisting of 90 residues forming five helices. This domain shows no structural similarity to any known protein structure. Apart from the common α-amylase B and C domains, it was also observed that AS contained an extra domain (termed B′) between β-strand 7 and α-helix 7 of the $(\beta/\alpha)_8$ domain. The absence of this domain in α-amylases led to speculations concerning a possible role of domain B′ in the transferase activity. The proposed catalytic residues of AS lie in the bottom of a pocket, a feature seen in other family 13 enzymes such as the hydrolase oligo-1,6-glucosidase (*12*). Other exo-acting hydrolases, for example, β-amylase (*13*) and glucoamylase (*14*), also exhibit this pocket architecture.

Since sucrose is an inexpensive and readily available D-glucose donor compared to the various nucleotide derivatives, the industrial potential of AS for synthesis of glucan, oligosaccharide, or glucoconjugates is large. For optimal utilization of the enzyme, targeting controlled synthesis of specific α-glucans starting from sucrose, it is necessary to minimize the side reactions. This requires a thorough analysis of the substrate binding and of the specificity-determining sites in the active site.

In this paper we describe the active site interactions between the native enzyme and a D-glucose molecule, as seen from a crystal structure of the complex at 1.66 Å. We also describe the interactions between the inactive active site mutant Glu328Gln and sucrose on the basis of the crystal structure at 2.0 Å. Both complexes give information on the substrate-binding mode. The sucrose complex shows how the substrate binds prior to catalysis, whereas the D-glucose complex mimics the covalent intermediate. These structures represent the first active site glycoside hydrolase complexes of these ligands reported.

[1] Abbreviations: Tris, tris(hydroxymethyl)aminomethane; EDTA, ethylenediamminetetraacetic acid; HEPES, 2-[4-(2-hydroxyethyl)-1-piperazinyl]ethanesulfonic acid.

MATERIALS AND METHODS

Expression and Purification. Expression and purification of the recombinant enzyme have been described by Potocki de Montalk et al. (*8*) and the mutant by Sarçabal et al. (*9*). Apart from the intended mutation the variant contains another substitution His131Tyr, as sequenced from the electron density. The proposed variant is possibly due to a PCR error. Comparison of the structures with and without (data not shown) sucrose shows that this mutation does not introduce any changes around the active site.

Crystallization and Data Collection. Crystals of recombinant and mutant AS were obtained by using the procedure previously described by Skov et al. (*11*, *15*). The crystallized AS lacks ten residues compared to the genomic sequence and contains four additional residues originating from the expression vector.

The protein in a concentration of 4−5 mg/mL and a volume of 2.5 μL was contained in a buffer consisting of 150 mM NaCl, 50 mM Tris-HCl, pH 7.0, 1 mM EDTA, and 1 mM α-dithiothreitol, mixed 1:1 and equilibrated against 500 μL of 30% (w/v) PEG 6000 and 100 mM HEPES, pH 7.0, using the hanging drop method at 4 °C. Large platelike crystals appeared within 2 weeks.

The D-glucose soaks were prepared by soaking the crystals (containing Tris bound in the active site) in solution containing the components of the reservoir and 14 mM D-glucose for 5 min, after which time the crystal was flash cooled using liquid nitrogen while mounted in a fiber loop. The crystals did not seem to suffer from the soaking in terms of physical damage or increase in mosaicity. Data collection was performed at ID-14 EH-1 (λ = 0.933 Å) at ESRF at 120 K, using a crystal to detector distance of 120 mm, oscillation range of 1.0°, and three passes of 5 s per frame.

The mutant crystals were grown with 14 mM sucrose in the reservoir solution and showed the same morphology as observed for the native crystals. The data on the sucrose cocrystallized crystal were collected at the MAX-LAB synchrotron radiation facility BL711 (λ = 1.106 Å) at 110 K, using a crystal to detector distance of 300 mm (large scan mode of a MAR 345 image plate), oscillation of 1.0° with one pass, and 180 s exposure per frame. Both data sets were processed using the HKL suite (*16*).

Structure Determination and Refinement. The crystals of both the D-glucose soak and the sucrose cocrystallization belonged to the space group $P2_12_12$ (one molecule per asymmetric unit) and had approximately the same cell dimensions as the native crystal (Table 1). Consequently, good preliminary phase estimates were readily available. All model building was performed using O (*17*) with SIGMAA (*18*) weighted $2mF_o - DF_c$ and $mF_o - DF_c$ density maps. Refinements were done with CNS (*19*) using the MLF target function in both cases. Validation of the models at various steps during refinement was done with PROCHECK (*20*). Analyses of the enzyme substrate interactions were done with LIGPLOT (*21*).

Data in the range of 13−1.66 Å were used, with bulk solvent correction and anisotropic scaling used at all refinement steps. From the beginning of the refinement 5% of the data was set side for cross-validation. Since there was clear density for the D-glucose in the active site, this was included from the start of the refinement. Initially, the structure was refined by rigid body refinement. Subsequently, three rounds of simulated annealing from 3000 K, followed by individual restrained *B*-factor refinement, were done. Water molecules were picked among spherical peaks of 1.5σ in the $2mF_o - DF_c$ map and were analyzed for hydrogen-bonding distances with the protein or other water molecules. In the structure are included 628 residues, 3 D-glucose molecules, and 890 water molecules. The final *R*-factor is 18.4% with an *R*-free of 20.2%, with 502 of the non-glycine residues lying in the most favorable, 50 in the additionally allowed, 2 in the generously allowed, and none in the disallowed regions of the Ramachandran plot. Clear density was seen throughout the structure. Ten residues were modeled in alternative conformations, and their occupancies were refined with CNS. None of the residues were close to the active site.

The relatively low completeness of the sucrose data set is due to ice formation in the drop during data collection. This resulted in excision of several reflections in resolution shells 4.31−3.42 Å and 2.25−2.15 Å, the completeness in those shells being 73% and 58%, respectively. The absence of these reflections leads to a slight distortion of the density map at some places. This is most evident when viewing the densities of aromatic residues, which in some cases are smeared.

The sucrose complex was refined using data in the range of 30−2.0 Å with protocols similar to those used for the D-glucose complex. Also here 5% of the data was set aside for cross-validation. In the structure are included 628 amino

Table 1: Data Collection Statistics[a]

	D-glucose	sucrose
space group	$P2_12_12$	$P2_12_12$
cell dimensions (Å)	a = 96.13	a = 95.59
	b = 116.73	b = 116.74
	c = 61.29	c = 60.83
resolution (Å)	13−1.66 (1.72−1.66)	30−2.00 (2.07−2.00)
total no. of reflections measured	619347	335382
no. of unique reflections	81373	39254
completeness (%)	99.3 (99.4)	84.2 (86.8)
$R(I)$[b] merge (%)	6.9 (33.8)	7.6 (19.7)

[a] Statistics for the highest resolution shell are given in parentheses. [b] $R(I) = \sum_{hkl}(\sum_i(|I_{hkl,i} - \langle I_{hkl}\rangle|))/\sum_{hkl,i}\langle I_{hkl}\rangle$, where $I_{hkl,i}$ is the intensity of an individual measurement of the reflection with Miller indicies h, k, and l and $\langle I_{hkl}\rangle$ is the mean intensity of that reflection.

Table 2: Refinement and Structure Quality Statistics for the D-Glucose and Sucrose Complexes

	D-glucose	sucrose
resolution (Å)	13−1.66	30−2.00
no. of protein atoms (residues 1−628)[a]	5072	5052
no. of solvent waters	890	622
no. of heteroatoms	36	23
R_{cryst}[b]	18.4	18.6
R_{free}[c]	20.2	22.6
rms deviation for bonds (Å)	0.008	0.005
rms deviation for angles (deg)	1.6	1.2
average protein *B*-value (Å^2)	19.47	11.04
average solvent *B*-value (Å^2)	29.14	20.65

[a] This discrepancy results from different modeling of alternative conformations in the two structures. The given statistics are calculated with the CNS package. [b] $R_{cryst} = \sum_{hkl}(||F_{o,hkl}| - |F_{c,hkl}||)/|F_{o,hkl}|$, where $|F_{o,hkl}|$ and $|F_{c,hkl}|$ are the observed and calculated structure factor amplitudes. [c] R_{free} is equivalent to the *R*-factor but calculated with reflections omitted from the refinement process (5% of reflections omitted).

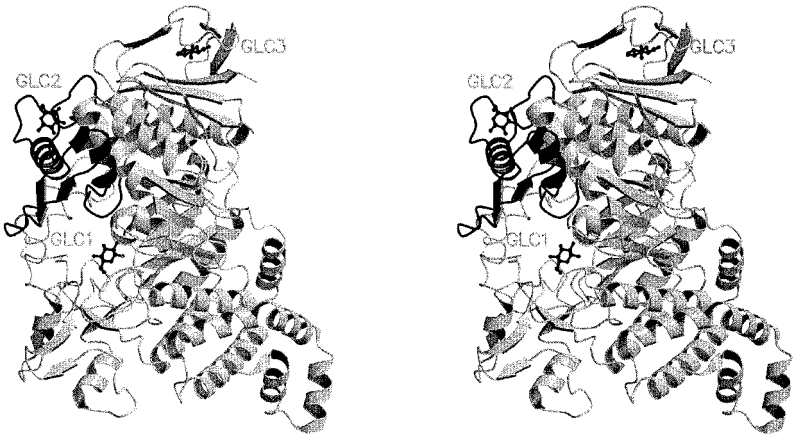

FIGURE 2: Stereoview of the fold of AS in a schematic representation, with the three D-glucose molecules (GLC 1, GLC 2, and GLC 3) shown in black. The B′ domain has been colored dark gray.

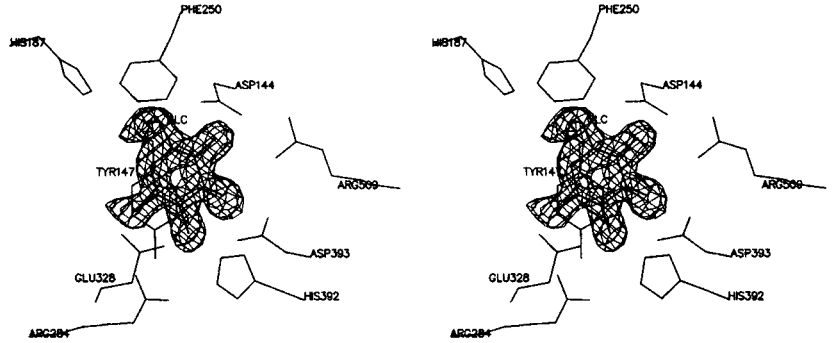

FIGURE 3: Stereoview of the simulated annealing $2mF_o - DF_c$ omit map of the active site of AS. The map has been contoured at 1.0σ around the D-glucose. The D-glucose and amino acid residues within 3.5 Å were omitted from the map calculation. Amino acid side chains involved in interactions with the D-glucose are shown.

acid residues, 1 sucrose molecule, and 634 water molecules. The final *R*-factor is 18.6% with an *R*-free of 22.6%, with 486 of the non-glycine residues lying in the most favorable, 68 in the additionally allowed, 1 in the generously allowed, and none in the disallowed regions of the Ramachandran plot. The electron density around the side chain of the mutated residue was weak, indicating that the Gln328 side chain can take several positions. The model only includes the residue in the major conformation. Gln328 is also disordered in the uncomplexed mutant structure (data not shown). The sucrose molecule shows very clear density; the sucrose was unambiguously fitted from the initial difference map.

Coordinates of both structures have been deposited in the Protein Data Bank, Rutgers, NJ, with the accession code 1jg9 for the D-glucose and 1jgi for the sucrose complex.

RESULTS AND DISCUSSION

D-Glucose Complex. The positions of two glucose molecules were clearly visible in the $mF_o - DF_c$ maps, with one bound in the active site pocket and one at the surface. Figure 2 shows a schematic representation of AS with bound glucose molecules, and Figure 3 shows a simulated annealing omit map of the active site.

The glucose (GLC 1 on Figure 2) in the active site was found to be the β-anomer, and it is in a $^4C_1$ conformation (*22*). This is the minimum energy conformation for glucose. Hence binding in the active site does not introduce any conformational strain in the glucose molecule, indicating that the pocket is optimized for this entity. The binding is at the proposed α-amylase −1 subsite, as mapped out by superposition of the AS structure and the TAKA-amylase−acarbose complex (*11*, *23*). The interactions between the glucose molecule and the enzyme are dominated by hydrogen bonds (of which some are water mediated), involving all of the glucose hydroxyl groups. Figure 4 shows in a schematic representation the residues involved in interactions with this glucose. These are primarily the conserved α-amylase active site residues Glu328, Asp393, His187, His392, and Arg284 (AS crystal structure numbering) (*8*). The observed hydrogen-bonding network confirms the roles of residues Asp393,

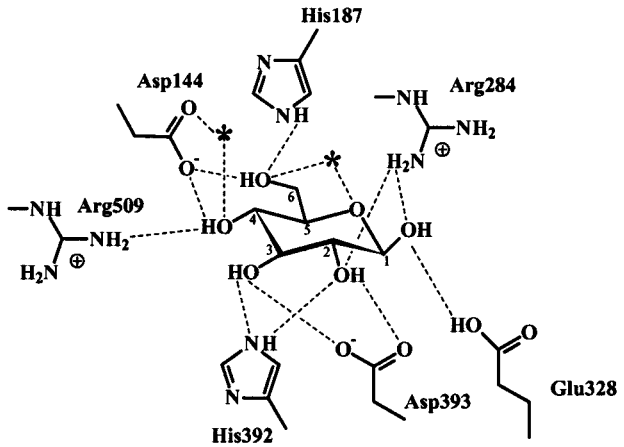

FIGURE 4: Schematic view of AS−D-glucose interactions with hydrogen bonds shown as dotted lines. Water molecules are marked as asterisks.

His187, His392, and Arg284 as hydrogen-bonding partners of the glucose moiety found at the −1 subsite in the α-amylase family. Residues Asp144 and Arg509 form a salt bridge that effectively converts the active site cleft found in α-amylases into the pocket topology observed in AS. Both residues are found in unconserved loop regions of AS (loops 2 and 7, respectively) (*11*), and both have interactions with the bound glucose molecule as shown in Figure 4. Glu328 (the general acid/base) OE1 hydrogen bonds to O1 with a distance of 2.6 Å. Since the bound glucose is the *β*-anomer, the catalytic nucleophile Asp286 points away from the glucose toward Asp144 where the distance between the respective OD2's is 2.7 Å. The O1 now occupies the position of the Asp286 OD1 seen in the Tris complex. Furthermore, Arg284 is pushed away from the position observed in the Tris complex structure. Glucose hydroxyl's O4 and O6 occupy the same position as Tris hydroxyl's O3 and O2 within the coordinate error. Furthermore, two water molecules found in the active site of the Tris complex has been displaced by glucose hydroxyl groups O2 and O3. This means that the overall enzyme hydrogen-bonding pattern does not change upon replacement of Tris with *β*-D-glucose.

Since the hydrogen bond interactions can at least equally well be satisfied through interaction with the solvent, the complex formation is likely to be associated with hydrophobic interactions. The glucose ring stacks on Tyr147, and this seems to be the main hydrophobic contact. Phe250, however, also stacks on the opposite side and interacts mainly with C6.

Since glucose is a 40%/60% mixture of α/*β*-anomer at the temperature of the soaking experiment, an obvious question is how the pocket is optimized for *β*-anomer binding. When an α-anomer is superimposed on the bound glucose, the only major difference in hydrogen bonding is that the O1 to Glu328 OE1 hydrogen bond is replaced by an O1 Glu328 OE2 hydrogen-bonding possibility. The latter is, however, less ideal in geometry, and the distance between donor and acceptor atoms is 2.9 Å, whereas the distance in the *β*-anomer complex is 2.6 Å. A minor difference is that a weak hydrogen bond between O1 and Arg284 NH1 is possible in the *β*-anomer but not in the α-anomer. These differences in interaction energies must be responsible for the *β*-anomer specificity. Notably in the intermediate (Figure 1) the covalently bound glucose is also in the *β*-conformation as found experimentally in the CGTase intermediate structure (*6*). It is possible to superimpose the active site residues of AS−glucose and CGTase−maltotriosyl (*6*). Doing this, the glucose and the covalently linked glucosyl of the maltotriosyl also superimpose within experimental error. This suggests that the active site of AS is optimized for the stabilization of the transition state and the structurally similar covalent glucosyl intermediate.

The AS−glucose structure shows an rms deviation of 0.144 Å over all 628 CA atoms from the Tris-complexed structure (*11*), so this change in ligand induces no major structural changes. Comparing the AS−glucose complex to the AS−Tris complex reveals a number of minor differences. The rings of Phe250 and Tyr147 are tilted slightly. His187 moves 0.2 Å toward the glucose O6, and because of the Tyr147 tilt Ile184 moves away from the Tyr ring. The carbonyl oxygens of His187 and Ile184 are hydrogen bonded to Tyr152 OH, and as a consequence of their movement Tyr152 moves approximately 0.4 Å. The change in position of Tyr152 in turn affects the conformation of the nearby Phe183, and several residues from the B domain move concertedly. The consequences of these changes are not clear, but a remote conformational change could be associated with the binding/release of the second substrate.

Flat and somewhat smeared $mF_o - DF_c$ density was found above the side chain of Phe417. This amino acid residue is positioned on the surface of AS, in the vicinity of the active site, but not in the substrate access channel identified previously (*11*). This density suggests an additional glucose-binding site (GLC 2). The distance from the aromatic Phe plane and the glucose ring plane is approximately 4.0 Å, which is within van der Waals interaction limits. In comparison, the equivalent distance between glucose and Tyr147 in the active site is approximately 3.7 Å. Phe417 is found in the unique AS insert from residue Asp394 to Glu460 between *β*-strand 7 and α-helix 7 of the barrel previously suggested to be involved in acceptor binding (*11*). Additionally, His414 is probably involved in hydrogen bonding to the surface glucose. In the vicinity two additional Phe residues, 421 and 425, are found, which could be involved in hydrophobic interactions with saccharides.

A well-defined third D-glucose molecule (GLC 3) is found between two symmetry-elated enzyme molecules. The major interactions are with residues Asn562 and Thr592 from the C-domain and with Asn258, Ser260, and Asn207 from the symmetry-related molecule B domain. The C-domain has in a previous case been shown to bind saccharides (*24*), but the site found in AS does not coincide.

Sucrose Complex with the Glu328Gln Mutant. The structure shows an rms deviation of 0.215 Å in CA positions from the Tris complex and 0.18 Å from the glucose-bound structure. Figure 5 shows the simulated annealing omit map at the sucrose-binding site. At the concentrations used in the cocrystallization only one sucrose molecule has been found complexed with the Glu328Gln mutant. It binds inside the active site with the glucosyl ring at the −1 position and the fructosyl moiety occupying subsite +1 using the sites mapped out from the superposition of AS (*11*) and the TAKA-amylase−acarbose complex (*22*). The +1 site is directly accessible from the solvent through the active site entrance channel. This indicates that AS only uses one active site entrance for both sucrose and the oligosaccharide chain to be elongated and only one active site saccharide binding site.

The conformation of the sucrose molecule can be described in terms of two dihedral angles: ϕ and ψ, ϕ being defined with O5, C1, O1, and C2′ and ψ with C1, O1, C2′, and O5′ (see Figure 6 for a schematic representation of sucrose; here, fructose atoms are labeled with a prime). In the Glu328Gln−sucrose complex the sucrose molecule adopts a conformation in which ϕ is 44° and ψ is −93°. The glucosyl ring is in an undistorted $^4C_1$ conformation, and the fructosyl ring is in an ^4E conformation. As can be seen from Figure 5, the electron density is very well defined, and it is obvious that sucrose is found in only one conformation.

The sucrose conformation observed in the active site can be compared to sucrose conformations found in sucrose crystals and to conformations based on theoretical calculations. The structures of sucrose from neutron diffraction studies (*25*) and X-ray analysis (*26*) show that the structure

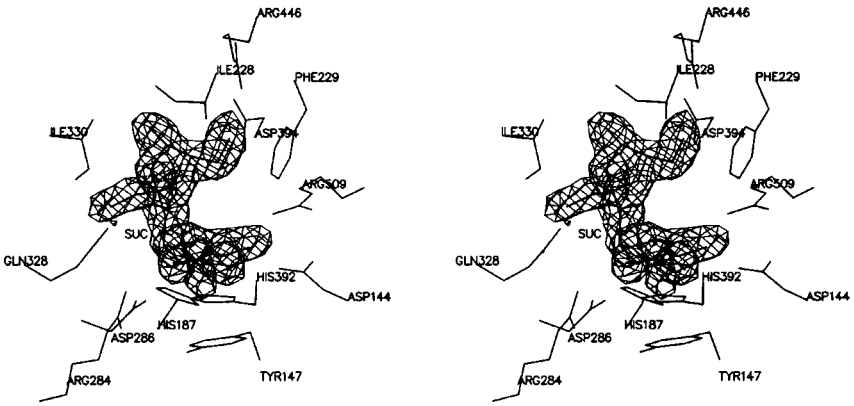

FIGURE 5: Stereoview of the simulated annealing $2mF_o - DF_c$ omit map of the active site of E328Q. The map has been contoured at 1.0σ around the sucrose. The sucrose and amino acid residues within 3.5 Å were omitted from the map calculation. Amino acid side chains involved in interactions with the sucrose are shown.

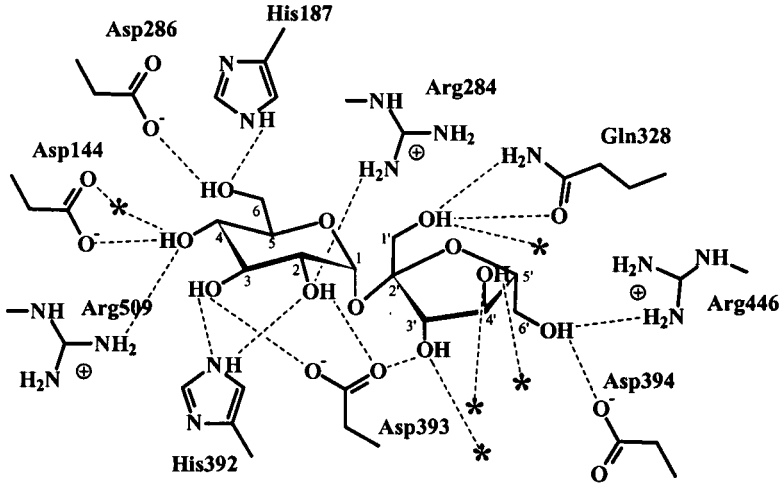

FIGURE 6: Schematic view of E328Q−sucrose interactions with the hydrogen bonds shown as dotted lines. Water molecules are marked as asterisks.

of the disaccharide is determined by two intramolecular hydrogen bonds, namely, between O2 and O1′ and between O5 to O6′ (Figure 6). The conformations of glucosyl and fructosyl rings in sucrose crystals are in $^4C_1$ and $^4T_3$, respectively. The conformational space of sucrose has also been studied by energy minimization and molecular dynamics methods (*27*). In terms of ϕ and ψ angles three main conformations, S1 (105.4°, −47.9°), S2 (80.4°, −170°), and S3 (80°, 60°), are found from vacuum studies, with both ring systems showing the same geometries as those found in the experimental studies. The ϕ and ψ angles of the S1 conformation are also very close to those observed in the crystalline systems, but only the O2 and O1′ hydrogen bond is found. In the molecular dynamics simulations, however, it was shown that no interresidue hydrogen bonds exist, since ideal hydrogen bonds can be obtained by a well-defined first hydration sphere. The ϕ and ψ angles found were those of the S1 conformation, but now with a water molecule as a mediator in the O2 and O1′ hydrogen bond in the crystalline state and in a vacuum. The simulations further showed that the $^4C_1$ conformation of the glucose is fairly rigid, whereas the fructose moiety displayed a large number of conformations with small but distinct minima around the ^4E and $^4T_3$ conformations.

The energy of the sucrose conformation we observe in the AS active site is well within the conformer distribution around the S1 conformation calculated in the sucrose/water molecular dynamics simulation (*27*). Hence, it can be concluded that AS does not impose a particularly strained conformation on sucrose upon binding.

The sucrose ϕ and ψ angles are affected by hydrogen bonds to Asp393, Asp394, and Arg446. Since Asp393 is conserved in the family 13 Asp394 and Arg446 (both located in the AS loop 7) (*11*) must be largely responsible for the fructosyl part of the substrate specificity. The main effect of the induced torsion angles is the alignment of the lone pair (lp) of the sucrose O1 with the acidic hydrogen of the wild-type enzyme Glu328. The almost linear O1:lp−H−O will minimize the proton-transfer energy barrier during catalysis or, in other words, stabilize the transition state toward the covalent intermediate (O1−Gln328 OE1 distance is 3.2 Å).

Binding of the glucose moiety is mediated by stacking with Tyr147 and Phe250 in addition to eight hydrogen bonds which are also found in the glucose complex (Figures 4 and 6): Asp144 OD2 to O4, His187 to O6, Arg284 NH2 to O2, His392 NE2 to O2 and O3, Asp393 OD2 to O2 and OD1 to O3, and Arg509 NH1 to O4. The nucleophile Asp286 lies in a different conformation than in the glucose complex, now forming a hydrogen bond to glucosyl−O6. All other active site side chains are at similar positions, including the mutated 328. This position of Asp286 is identical to that found in

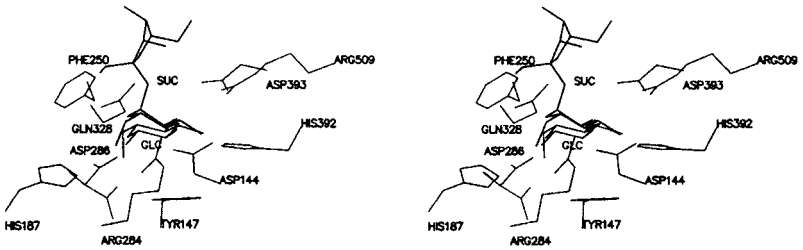

FIGURE 7: Superposition of the active sites of the AS−glucose and AS−sucrose complexes. Only Asp286 with very different positions in the two complexes is shown in both conformations. The glucose molecule is found at the same position as the glucosyl ring of the CGTase−glucosyl intermediate (*6*). The position of the glucosyl ring of the sucrose molecule is close to that of the glucosyl ring in the −1 position of the CGTase−maltononaose complex (*6*). These similarities emphasize the active site stabilization of the covalent intermediate.

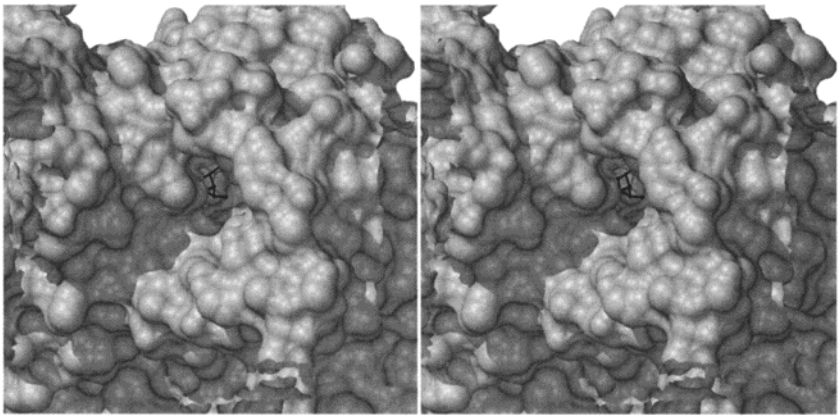

FIGURE 8: Stereoview of the substrate access channel with sucrose bound. Sucrose is seen to effectively block the access with the fructosyl ring occupying the +1 subsite. No other channels leading to the active site can be located. Formation of other channels would require structural rearrangements.

the Tris complex, a position enabling it to participate in the catalytic mechanism. The AS−glucose and AS−sucrose complexes are superimposed in Figure 7. When the positions of the two glucosyl rings are compared, it can be seen that the major difference in position can be described as a 20° rotation and a small translation. The rotation is around the C3−C4 bond with the sucrose glucosyl moiety being rotated away from coplanarity with the Tyr147 side chain. The major differences in atomic positions are therefore observed for atoms C1 and O5. Both pairs are about 1.1 Å apart. The observed position of the sucrose glucosyl moiety superimposes well with the glucosyl moiety at the −1 position of the CGTase−maltononaose complex (*6*). So with respect to substrate−enzyme interactions at the −1 subsite, AS and CGTase appear to be very similar.

Since glucose was found to bind at the same position as the covalently linked glucose ring of the CGTase−maltotriosyl complex, the following theory can be put forward: The substrate −1 ring (represented by the Glu328Gln−sucrose and the CGTase−maltononaose structures) is bound with poorer hydrophobic interactions as compared to those that can be achieved in the covalent intermediate (represented by AS−glucose and the CGTase−maltotriosyl structures), and this introduces a driving force for the catalyzed reaction.

Whereas only one water molecule associates to the pyranosyl ring of sucrose by hydrogen bonding to O4, four direct and four water-mediated hydrogen bonds are seen in the fructosyl moiety interactions with AS (see Figure 6). These water molecules are again hydrogen bonded to AS residues that are not conserved in the family, and they are situated in the substrate access channel. This probably reflects that the fructose has to be able to easily exit the pocket during the catalytic cycle. Attempts to make complexes of fructose with native AS have not been successful, as no fructose on either furanosyl or pyranosyl form can be seen in the structure (data not shown).

Reaction Catalysis. Since the function of AS is the elongation of existing polymers as demonstrated by the kinetic investigations in the presence of glycogen (*1*), the AS−sucrose complex gives information on the first steps of the reaction mechanism outlined in Figure 1. Glu328 is first functioning as an acid by initially protonating the glycosidic bond of the sucrose molecule aligned for optimal transfer via interactions with the enzyme. The direct enzyme interactions with the fructosyl ring are the hydrogen bonds to residues Asp394 and Arg446, respectively; the interactions to the glucosyl moiety are, with the exception of the salt bridge (Asp144−Arg509), similar to those seen between α-amylases (*23*) and glucosyl moieties at the −1 position of the active site. Glu328 is later serving as general base to activate the incoming nucleophile for attack on C1. Asp286 serves as the catalytic nucleophile by attacking C1. It hereby assists leaving group departure and hereafter forms a covalent enzyme intermediate. The distance between Asp286 OD1 and C1 of sucrose is 3.1 Å, a distance short enough to make a nucleophilic attack possible. The D-glucose moiety stacks on Tyr147, this again rests on Pro134 [structurally conserved in the closely related TAKA-amylase (*28*) and oligo-1,6-glucosidase (*12*)], and the position of Tyr147 is further stabilized by an OH hydrogen bond to Asp182 and to Arg205 NH1.

The similarities between AS and α-amylases in active site/substrate interactions observed in AS strongly suggest that the mechanism up to the formation of the covalent interme-

diate is the same. However, AS needs an activated first substrate (sucrose) compared to the hydrolases. This probably reflects the loss of entropy of the entire catalyzed system upon the formation of long chains.

The information on the next steps of the reaction that can be obtained from the complexes is more indirect and speculative. Upon complex formation with sucrose (using concentrations around 20 mM) only one binding site is observed. In this binding site sucrose effectively blocks the active site access channel (*11*); in particular, the α-amylase +1 subsite is occupied by the fructosyl ring. As there are no other channels open to the active site (Figure 8), major structural changes are required to establish an alternative +1 site. Such changes are not induced by the formation of the complex with either sucrose or glucose, but the effect of the presence of a longer oligosaccharide (an acceptor) is unknown. Unfortunately, the two-substrate kinetic data available is not unambiguously assigning either ordered or ping-pong-type steady-state kinetics (*1*), making the following hypothetical. Assuming that no major structural changes occur leads to the suggestion of ping-pong-type kinetics: Sucrose enters the active site, a covalent intermediate is formed, and fructose is released out through the channel where subsequently the second substrate (glycogen) enters, reacts with the covalent intermediate, and finally exits the active site to allow for the entrance of the next sucrose molecule. This mechanism would, however, make the control of hydrolysis very difficult to envisage. AS *is* able to control hydrolysis effectively. In the presence of glycogen, hydrolysis is negligible, and it is only a minor side reaction in the absence of the second substrate (*2*). The problem with control of hydrolysis in transferase reactions is well-known and discussed in the analysis of other glycosyltransferases (*29*, *30*). These studies suggest that another mechanism involving significant structural changes is likely.

The only circumstantial information on acceptor binding comes from the second D-glucose-binding site (GLC 2 on Figure 2) seen in the D-glucose complex. This glucose may well occupy a subsite of an external polysaccharide-binding site. Hopefully, further work will make complexes with acceptor oligosaccharides available and lead to an understanding of the latter steps in the AS reaction mechanism.

ACKNOWLEDGMENT

We thank Mette B. Hersom for help with the crystallization experiments.

REFERENCES

1. Potocki de Montalk, G., Remaud-Simeon, M., Willemot, R., and Monsan, P. (2000) *FEMS Microbiol. Lett. 186*, 103−108.
2. Potocki de Montalk, G., Remaud-Simeon, M., Willemot, R. M., Sarçabal, P., Planchot, V., and Monsan, P. (2000) *FEBS Lett. 471*, 219−223.
3. Henrissat, B., and Davies, G. (1997) *Curr. Opin. Struct. Biol. 7*, 637−644.
4. Yoshioka, Y., Hasegawa, K., Matsuura, Y., Katsube, Y., and Kubota, M. (1997) *J. Mol. Biol. 271*, 619−628.
5. Mosi, R., He, S. M., Uitdehaag, J., Dijkstra, B. W., and Withers, S. G. (1997) *Biochemistry 36*, 9927−9934.
6. Uitdehaag, J. C., Mosi, R., Kalk, K. H., van der Veen, B. A., Dijkhuizen, L., Withers, S. G., and Dijkstra, B. W. (1999) *Nat. Struct. Biol. 6*, 432−436.
7. Davies, G., and Henrissat, B. (1995) *Structure 3*, 853−859.
8. Potocki de Montalk, G., Remaud-Simeon, M., Willemot, R. M., Planchot, V., and Monsan, P. (1999) *J. Bacteriol. 181*, 375−381.
9. Sarçabal, P., Remaud-Simeon, M., Willemot, R., Potocki de Montalk, G., Svensson, B., and Monsan, P. (2000) *FEBS Lett. 474*, 33−37.
10. Henrissat, B., and Bairoch, A. 1996 *Biochem. J. 316*, 695−696.
11. Skov, L. K., Mirza, O., Henriksen, A., Potocki de Montalk, G., Remaud-Simenon, M., Sarçabal, P., Willemot, R. M., Monsan, P., and Gajhede, M. (2001) *J. Biol. Chem.. 276*, 25273−25278.
12. Watanabe, K., Hata, Y., Kizaki, H., Katsube, Y., and Suzuki, Y. (1997) *J. Mol. Biol. 269*, 142−153.
13. Oyama, T., Kusunoki, M., Kishimoto, Y., Takasaki, Y., and Nitta, Y. (1999) *J. Biochem. 125*, 1120−1130.
14. Aleshin, A., Golubev, A., Firsov, L. M., and Honzatko, R. B. (1992) *J. Biol. Chem. 267*, 19291−19298.
15. Skov, L. K., Mirza, O., Henriksen, A., Potocki de Montalk, G., Remaud-Simeon, M., Sarçabal, P., Willemot, R. M., Monsan, P., and Gajhede, M. (2000) *Acta Crystallogr. D56*, 203−205.
16. Otwinowski, Z. (1993) in *Proceedings of the CCP4 study weekend: Data collection and processing*, pp 56−62, SERC Daresbury Laboratory, Warrington, U.K.
17. Jones, A., Zou, J. Y., Cowan, S. W., and Kjeldgaard, M. (1991) *Acta Crystallogr. A47*, 110−119.
18. Read, R. J. (1986) *Acta Crystallogr. A42*, 140−149.
19. Brunger, A. T., Adams, P. D., Clore, G. M., DeLano, W. L., Gros, P., Grosse-Kunstleve, R. W., Jiang, J. S., Kuszewski, J., Nilges, M., Pannu, N. S., Read, R. J., Rice, L. M., Simonson, T., and Warren, G. L. (1998) *Acta Crystallogr. D54*, 905−921.
20. Laskowski, R. A., MacArhur, M. W., Moss, D. S., and Thornthon, J. (1993) *J. Appl. Crystallogr. 26*, 283−289.
21. Wallace, A. C., Laskowski, R. A., and Thornton, J. M. (1995) *Protein Eng. 8*, 127−134.
22. Lindhorst, T. K. (2000) *Essentials of Carbohydrate Chemistry and Biochemistry*, Wiley-VCH, Weinheim.
23. Brzozowski, A. M., and Davies, G. J. (1997) *Biochemistry 36*, 10837−10845.
24. Dauter, Z., Dauter, M., Brzozowski, A. M., Christensen, S., Borchert, T. V., Beier, L., Wilson, K. S., and Davies, G. J. (1999) *Biochemistry 38*, 8385−8392.
25. Brown, G. M., and Levy, H. A. (1973) *Acta Crystallogr. B*29, 790−797.
26. Hanson, J. C., Sieker, L. H., and Jensen, L. H. (1973) *Acta Crystallogr. B*29, 797−808.
27. Immel, S., and Lichtenthaler, F. W. (1995) *Liebigs Ann.*, 1925−1937.
28. Matsuura, Y., Kusunoki, M., Harada, W., and Kakudo, M. (1984) *J. Biochem. 95*, 697−702.
29. Persson, K., Hoa, L. D., Dieckemann, M., Wakarchuk, W. W., Withers, S. G., and Strynadka, N. C. J. (2001) *Nat. Struct. Biol. 8*, 166−175.
30. Charnock, S. J., and Davies, G. J. (1999) *Biochemistry 38*, 6380−6385.

BI010706L